Testing a mechanistic soil erosion model with a simple experiment

A. Heilig[a], D. DeBruyn[b], M.T. Walter[c], C.W. Rose[d], J.-Y. Parlange[a], T.S. Steenhuis[a,*],
G.C. Sander[e], P.B. Hairsine[f], W.L. Hogarth[d], L.P. Walker[a]

[a]*Department of Agricultural and Biological Engineering, Cornell University, Ithaca, NY 14853, USA*
[b]*Department of Mathematics, Bowie State University, Owings, MD 20736, USA*
[c]*Environmental Science, University of Alaska Southeast, Juneau, AK 99801, USA*
[d]*Faculty of Environmental Science, Griffith University, Nathan, Qld 4111, Australia*
[e]*Department of Civil and Building Engineering, Loughborough University, Loughborough, LE11 3TU UK*
[f]*CSIRO Land and Water, P.O. Box 1666, Canberra ACT 2601, Australia*

Abstract

A simple experiment was used to test the development of a "shield" over the original soil and associated changes in sediment concentrations as described in the mechanistic Rose erosion model. The Rose model, developed for rain-induced erosion and sediment transport on hillslopes (J. Hydrol., 217 (1999) 149; Trends Hydrol., 1 (1994) 443), was applied to a simple experimental set-up, consisting of a small horizontal soil surface (7×7 cm^2) under constant shallow (5 mm) overland flow with raindrop impact. The soil consisted of two particle size classes, clay and sand, greatly simplifying the analytical solution of the Rose model by reducing the unknown system parameters to one, the soil detachability. Photographic documentation of shield formation corroborated the conceptual validity of the Rose model. Using a single, best-fit value for the soil detachability, quantitative agreement between modeled and experimental results is excellent ($R^2 = 0.9$). This research provides lucidity to the primary processes enveloped in the Rose model and these mechanisms can be extrapolated to more complicated or realistic systems in which the individual processes may be more difficult to recognize. © 2001 Elsevier Science B.V. All rights reserved.

Keywords: Soil erosion; Rose model; Shield formation; Soil detachment; Rainfall impact; Deposition

1. Introduction

Though, after half a century of study, water-induced soil erosion mechanisms continue to stir controversy, it is widely recognized that upland erosion is largely initiated by the impact of raindrops on the soil surface. Recently, Hairsine and Rose (1991) and Rose et al. (1994) developed a physically based model of rain impact soil erosion on a hillslope,

the Rose model. The conceptual model proposed by Hairsine and Rose (1991) and Rose et al. (1994) addresses the situation where the shear forces of overland flow are insignificant and surface runoff merely transports sediment entrained into the flow by the energy of falling raindrops. Since the Rose model has only been tested against a limited amount of experimental data (Proffitt et al., 1991), the objective of our research was to perform additional experiments to test further the underlying physical processes of the model.

Central and unique to the Rose model is the development of a "shield" composed of relatively heavy

---

* Corresponding author. Tel.: +1-607-255-2489; fax: +1-607-255-4080.

E-mail address: tss1@cornell.edu (T.S. Steenhuis).
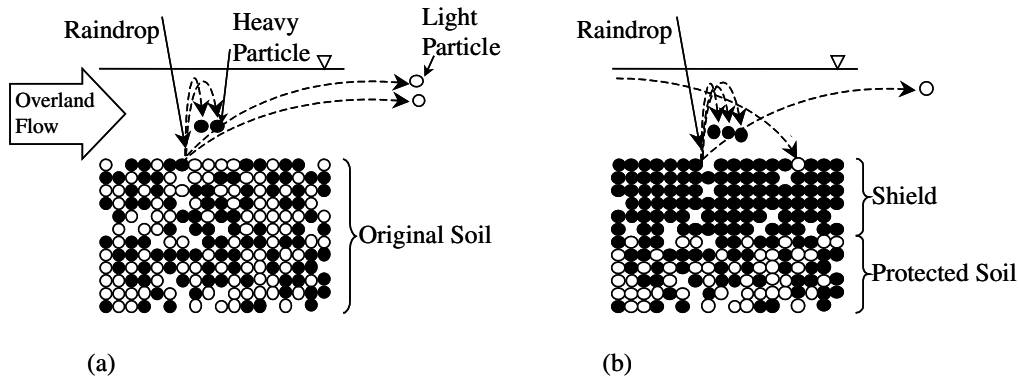
Fig. 1. Schematic of soil shield development from (a) initial rain impact to (b) well developed shield.

soil particles that protects the underlying soil from rain impact erosion. A conceptual description of the process is illustrated in Fig. 1. When a soil surface is initially inundated with raindrops, soil particles are detached from the soil surface and entrained into the overland flow (Fig. 1a). Light particles, with low settling velocities, will move far from their original point of dislodgment and heavy particles will settle quickly, near their original positions. If this process continues, eventually most of the lighter particles will be removed, leaving a *shield* of heavier particles that protect the underling soil (Fig. 1b). The full process obviously involves deposition, reattachment, and many soil-size classes or distribution functions and is fully described in published papers by Hairsine and Rose (1991), Rose et al. (1994, 1998), Sander et al. (1996) and Parlange et al. (1999).

Laboratory experiments demonstrating the model's conceptual basis (Proffitt et al., 1991) have been compared to analytical/numerical solutions of the model by Sander et al. (1996) and Parlange et al. (1999) and have shown strong agreement between model results and experimental data. However, the experiments were, in many ways, too complicated to elucidate the fundamental conceptual model; e.g. the roles of interdependent parameters were difficult to ascertain from the experiments alone. This study investigates the formation and protective nature of the surface shield that was not easily observed or measured in the Profitt et al. (1991) tilted-flume experiments. On sloped surfaces (e.g. Profitt et al., 1991) the entrained particles, even the heaviest, continuously jump downslope so that the hillslope is

never fully protected. Our experimental set-up employs a horizontal surface so that the heaviest particles do not leave the system and full protection, or "shielding," eventually develops. To simplify the testing but still maintain the ability to test the physical processes, two size particles were used, clay, which once entrained into the flow never settles, and sand which settles very rapidly. Other simplifications include constant depth and no spatial dependence on the overland flow rate.

2. Experimental methods

The laboratory experiments were designed to check the conceptual Rose model and be as simple as possible so that there was no ambiguity in the processes or their interpretation. The rainfall rate was varied; all other parameters were kept as constant as possible. The experimental set-up is schematically diagramed in Fig. 2. A small, Plexiglas cube ($7 \times 7 \times 7 \text{ cm}^3$) was filled with an artificial soil and leveled under a rainmaker. After carefully establishing an initial pond depth of 5 mm on the soil, rain was simulated over the box and an overflow spout in the side of the box maintained constant ponding depth (Fig. 2). Four experiments were run at different rain rates (35–100 mm h^{-1}). Two runs were made at 100 mm h^{-1} to show the characteristic scatter of the data when the experiments were duplicated. Outflow was periodically collected from the overflow spout with an automatic fraction sampler. In the first stage of each experiment, samples were collected every 15–30 s
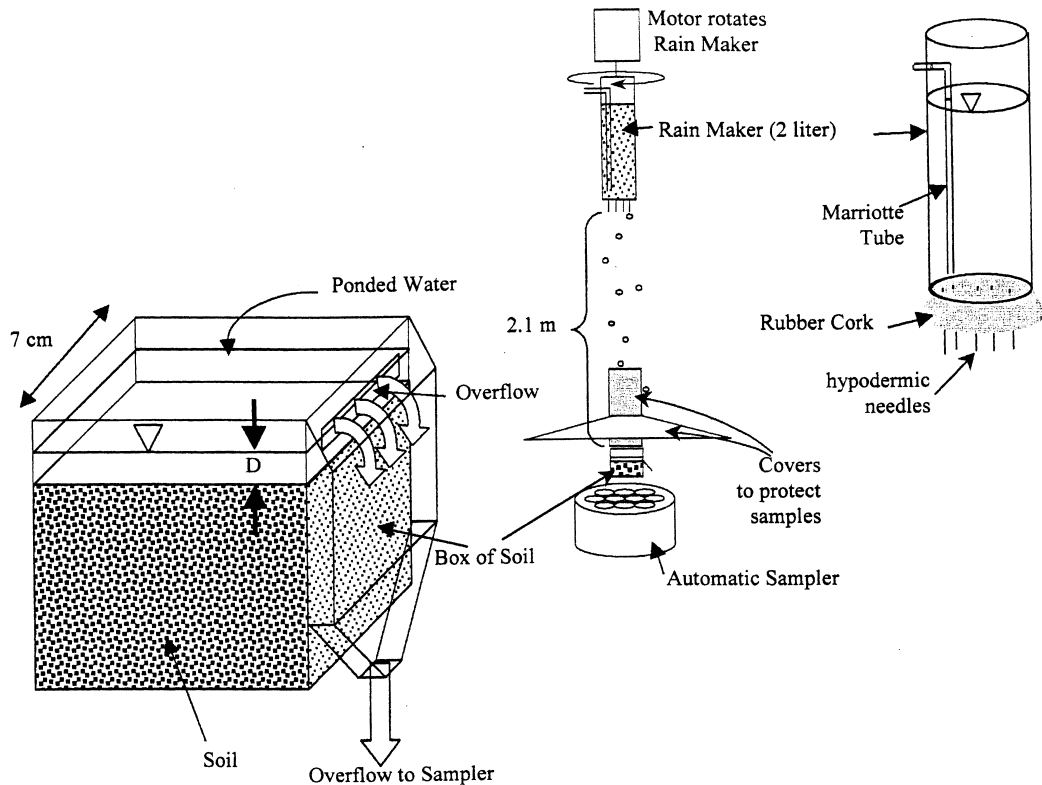
Fig. 2. Schematic of experimental set-up.

(depending on the rainfall rate), later, samples were collected at longer intervals. Each experiment continued until the ponded water was completely clear, 1.5–5 h, depending on the rainfall rate. The sediment concentration of each sample was measured using a spectrophotometer (Bausch and Lomb, Spectronic 1001, 546.1 nM wavelength). In these experiments, distilled water was always used.

The soil, 90% sand (180–212 m) and 10% clay (hydrous Kaolin supplied by Englehard Corp, NJ), was prepared as a saturated mixture in order to minimize clay aggregation. The saturated mixture was then put into the Plexiglas cube and placed under the rainmaker where the soil surface was smoothed and leveled. Pre-ponding was achieved by placing a strip of paper on the soil surface to prevent erosion. Water was carefully pipetted onto the paper to a depth of 5 mm at which time the paper was removed with minimal disturbance to the soil. The rainmaker was then turned on and a timer started simultaneously.

Rain was simulated using a 20 cm diameter, water-filled Marriotte cylinder rotating at about 20 rpm. The bottom end of the cylinder was pierced by hypodermic needles (B-D[®]21g1.5). The rainmaker was placed near the ceiling of the laboratory, 2.1 m above the soil cube. The rain rate was increased or decreased by the addition or removal of needles but the size of individual drops remained constant (~1.7 mm radius). Needle distribution was determined by trial and error until a uniformity of 85% or greater was achieved. Uniformity was determined using nine vials (1.5 cm diameter) evenly distributed over the soil cube position. Though the raindrops probably did not reach terminal velocity, the calculated rain energy was similar to that of the Proffitt et al. (1991) experiments, 22.8 J m^{-2} for 1 mm of rain. Note that though natural rainfall is characterized by different sized and speed raindrops, we strived for uniform raindrop characteristics. By doing so, we eliminated complexities arising from a distribution

of rain-impact characteristics and uncertainties from additional "curve-fitting." If this experiment was to be used to measure soil detachability for natural rainfall, more realistic rainfall would be needed.

Upon completion of each experimental run, the samples were diluted to fit into the range of the spectrophotometer calibration curve made prior to the experiment. The calibration curve was developed by correlating a set of solutions of known clay concentration to respective optical density (OD) readings. The calibration curve had an R^2 of 0.995 and an error of less than 4%.

3. Model derivation and parameterization

Following the derivation by Sander et al. (1996), each particle class represents an equivalent mass. Consider a soil composed of nine parts sand to one part clay by mass. To apply the model to this medium, the soil is divided into 10 classes, one class of clay and nine identical classes of sand

$$
\left.
\begin{aligned}
i &= 1 & \text{clay} \\
i &= 2, 3 \ldots 10 & \text{sand}
\end{aligned}
\right\} \tag{1}
$$

The different classes are characterized by their concentrations in the suspension, c [M L^{-3}] and by their masses per unit area in the deposited layer, M_d [M L^{-2}]. The settling velocity of the clay particles is slow, and within a limited time scale, is negligible, i.e. essentially zero. In contrast, the sand particles settle very quickly and are primarily found in the deposited layer.

$$
\begin{aligned}
c_1 &\neq 0; & M_{d1} &= 0 \\
c_{i=2,3\ldots10} &= 0; & M_{di=2,3\ldots10} &\neq 0
\end{aligned} \tag{2}
$$

For this simple scenario, Eq. (9) of Sander et al. (1996) can be written for the clay fraction as

$$
\frac{dc_1}{dt} = \frac{1}{D}\left[\frac{aP}{I}(1 - H) - Pc_1 \right] \tag{3}
$$

where c_1 is the concentration of clay in the surface flow [M L^{-3}], D the flow depth [L], P the rainfall rate [L T^{-1}], and I the number of particle size classes characterizing the soil (i.e. $I = 10$); each class represents an equivalent mass fraction. The parameter a is the bare soil's detachability [M L^{-3}]. The term Pc_1, is the

mass flow rate of clay particles out of the system. H represents the shielding state of the soil. A shielding state, $H = 0$, corresponds to no shield and $H = 1$ to complete shielding and full protection from further erosion. The original model addresses the additional process of redetachment of deposited material; the scenario investigated here does not involve this process. In the scenario described here, the hypothesis is that the clay erodes away and a sand deposition layer accumulates to shield the underlying soil.

The total mass per unit area of sand in the deposited or shield layer is $M_d = \sum_{i=2}^{10} M_{di}$. Following Sander et al. (1996) the sand fraction can be expressed as

$$
\frac{dM_d}{dt} = 9\frac{aP}{10}(1 - H) \tag{4}
$$

The shield H is expressed as (Sander et al., 1996)

$$
H = \frac{M_d}{M_d^*} \tag{5}
$$

where M_d^* is the total mass of the deposited material per unit area (sand) in the shield once it is complete.

Eq. (4) can be solved using the initial condition $M_d = 0$ at $t = 0$ to yield

$$
M_d = M_d^*\left[1 - \exp\left(-\frac{9aP}{10M_d^*}t \right) \right] \tag{6}
$$

Substituting Eq. (6) into Eq. (5), the formation of the shield H is

$$
H = 1 - \exp\left(-\frac{9aP}{10M_d^*}t \right) \tag{7}
$$

The parameter M_d^* can be replaced by the total mass of eroded particles, $9M_1^*$, since the ratio of masses in the original soil is known; i.e. $(M_d^*/M_1^*) = 9$. The mass per unit area of clay removed from the original soil, M_1^*, can be calculated by integrating the product of measured clay concentration in the suspension (c_1) and the flux, which for our steady state experiments is the rain rate, P

$$
M_1^* = \int_0^\infty c_1 P \, dt \tag{8}
$$

Inserting the expression for H in Eq. (7) into Eq. (3) yields a linear first-order equation for which, using the

Table 1
Experimental parameters and statistics

Parameters	Values			
	Run 1	Run 2	Run 3	Run 4
P (mm h^{-1})	35	60	100	100
M_1^* (mg cm^{-2})	70	74	75	85
R^{2}[a]	0.91	0.85	0.91	0.97
RD[b] (%)	22	27	18	11

[a] Correlation coefficient for predicted vs. observed concentrations.

[b] Relative difference between predicted and observed concentrations: (standard error/mean).

initial condition $c_1 = 0$ at $t = 0$, the solution is

$$c_1(t) = \exp\left(-\frac{P}{D}t\right) \frac{\dfrac{a}{10D}}{\dfrac{1}{D} - \dfrac{a}{10M_2^*}}$$

$$\times \left[\exp\left[\left(\frac{1}{D} - \frac{a}{10M_1^*}\right)Pt\right] - 1 \right] \qquad (9)$$

Comparison among experiments can be streamlined via normalized, dimensionless parameters.

Consider the following dimensionless variables:

$$C = c_1\frac{D}{M_1^*}, \ T = t\frac{P}{D}, \ \text{and} \ \lambda = \frac{a}{10}\frac{D}{M_1^*} \qquad (10)$$

From the definitions in Eq. (10), a simple relationship between the dimensionless concentration variable, C, and the dimensionless time variable, T, can be obtained

$$C(T) = \frac{\lambda}{1-\lambda}[\exp[(1-\lambda)T] - 1]\exp(-T) \qquad (11)$$

If preparation of the soil is identical for all experiments, a, the soil detachability will be the same; and if the raindrops are identical as well, M_1^* will also be the same. Thus, all observations among experiments with different Ps should be identical for the dimensionless variables; i.e. ideally, the C versus T curves superimpose themselves on one another for all experiments regardless of P.

4. Results and discussion

Table 1 summarizes the results. The R^2 values were consistently near 0.9, indicating good general correlation between predicted and observed sediment concentrations, $c(t)$. The relative difference was consistently
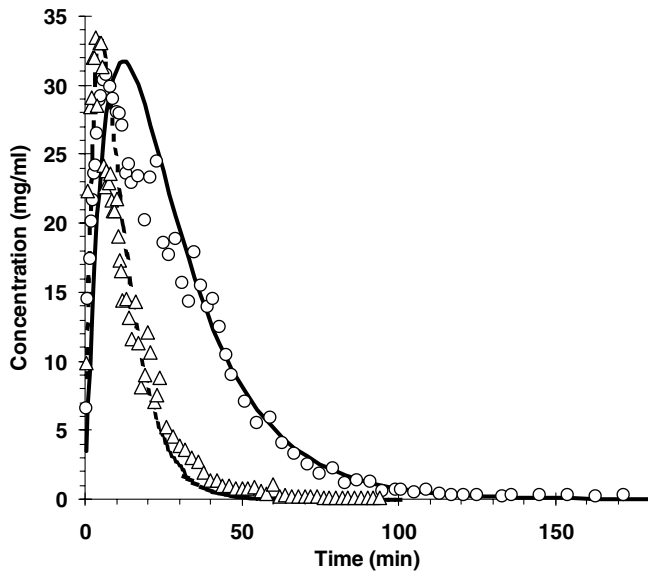
Fig. 3. Temporal concentration changes: circles, $P = 35$ mm h^{-1} (run 1); triangles, $P = 100$ mm h^{-1} (run 4); see Table 1 for other parameters associated with each run.
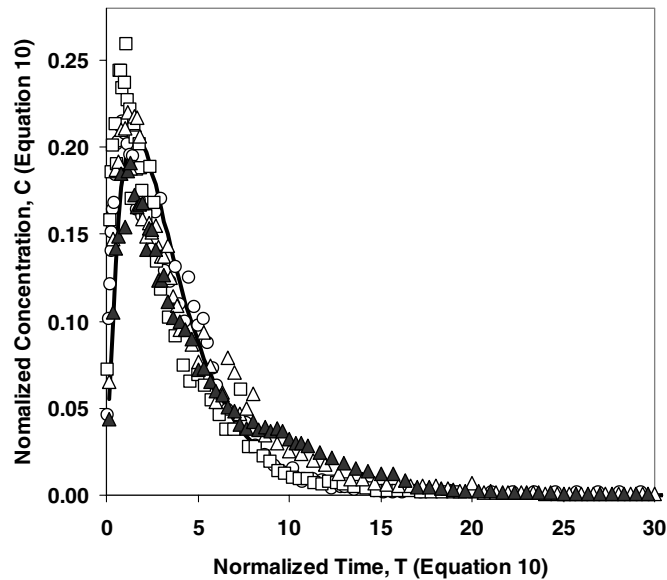
Fig. 4. Comparison between observed and theoretical $C(T)$; composite $R^2 = 0.93$. Each symbol is a unique experimental run (Table 1): circles, run 1; squares, run 2; solid triangles, run 3; open triangles, run 4. The line shows the model.

near 20%, also indicating good model predictability. The total mass of eroded material, M_1^*, was determined by integrating the data over time and was relatively consistent with <20% variation. The detachability, a, of a Solonchack soil determined by Proffitt et al. (1991), ~50 mg cm^{-3}, was an order of magnitude lower than determined for the artificial soil used in this study ~540 mg cm^{-3}. Such differences in soil parameters can be explained by the unique and unnatural condition of the soil. The detachability was determined by fitting Eq. (11) to the cumulative data from all four experiments; detachability considering individual experiments ranged from 438 to 686 mg cm^{-3}.

During the experiments, the impact of drops near the walls of the soil chamber was easily observed. In agreement with Rose's conceptual model, each drop acted as a little "shovel", ejecting all material, sand and clay, from the soil surface and dispersing it through the water layer. For the briefest moment after a drop's impact, a small crater was visible and quickly filled with settling particles and debris from neighboring drop impacts.

Fig. 3 shows the agreement between the Rose model (Eq. (9)) and the raw data and for the extreme-end rain rates, $P = 35$ mm h^{-1} (run 1) and

$P = 100$ mm h^{-1} (run 4). To avoid clutter, only two experimental runs are shown. The trends agree with the model theory. Initially, the concentration increases with time as clay is eroded from the soil and the rate of erosion decreases as the shield forms. Eventually, the shield protects the soil enough that the erosion rate is sufficiently slowed such that the temporal trend in concentration is reversed; the concentration of clay in suspension decreases because more clay is leaving in the overland flow than is being eroded from the soil. In our special case of a level soil surface, the shielding approaches completeness; this claim is corroborated by the fact that the clay concentrations go to approximately zero for long times. The attenuated curve for the lower rain rate is expected. The short- and long-time behaviors are in total agreement with observations of more complex systems (Sander et al., 1996; Parlange et al., 1999). Note that the peak concentrations in Fig. 3 for the two curves are similar even though the rain rates differ by nearly a factor of three. This may at first seem counterintuitive but is supported by both Rose's conceptual model and the experimental data.

Fig. 4 succinctly shows agreement between the Rose model (Eq. (11)) and normalized observations (Eq. (10)) for all experiments ($R^2 = 0.93$). As shown
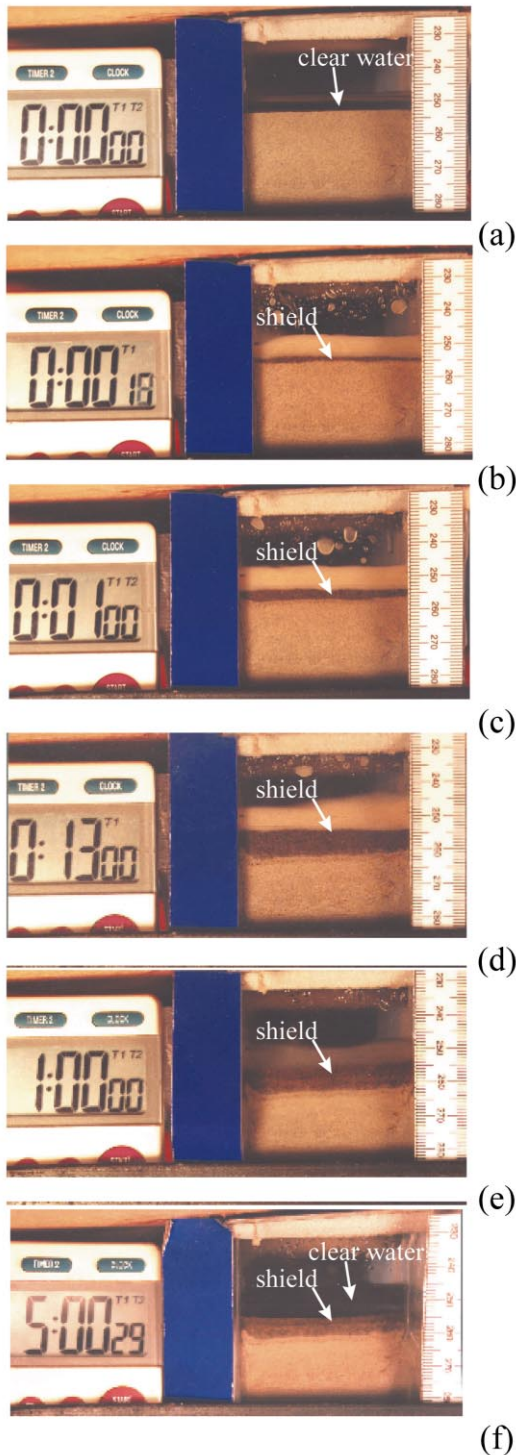
Fig. 5. Photographs of shield formation. Vertical scale in cm; time in h:min:s.

in Table 1, the total mass of eroded material is similar for all experiments regardless of rain rate. There is a slight systematic increase in M_1^* with increasing rain rate (Table 1); the systematic trend is also visible in the curves' tails shown in Fig. 4. The authors hypothesize that this arises because of the momentary suspension of sand particles upon raindrop impact; this action keeps a portion of the shield in suspension, thus reducing its effectiveness in protecting the underlying soil. Slightly better results may be obtained by employing a finite settling velocity for the sand particles rather than the "instantaneous" settling assumed here.

There is also a slight but systematic deviation between the observation and model apparent in Fig. 4; namely the model reacts faster than the experiments up to $T = 5$ and lags the experimental data for $T > 5$. The underestimation by the model for long time periods is probably due to continuous resuspension and escape of some of the shield materials which are ignored in the model; this is supported by the increasing trend in discrepancy with increasing rain intensity. It may also arise from interactions between raindrops in the experiments violating the implied assumption that the raindrops act independently. The probability of raindrop interactions would also increase with rain intensity. Reasons for the short time discrepancies may arise from the overly simplified expression for H (Eq. (5)); this is the basis for current ongoing studies by the authors. Regardless of the physical reasons, these minor discrepancies illustrate the complexities involved in soil erosion, even for these seemingly trivial experiments.

The dynamic formation of the shield during an experiment is illustrated in Fig. 5. The shield is clearly visible as the dark layer of sand at the surface of the soil in Fig. 5a–f. Notice how quickly the shield develops, it is clearly visible after 18 s (Fig. 5b). Within the first 5–10 min, the shield is nearly complete and does not grow significantly over the next several hours. This qualitatively agrees with model solutions in previous studies, especially Parlange et al. (1999). It is also obvious from the clear water in Fig. 5f, compared to Fig. 5b and c, that the shielding is complete, halting erosion. The water is also clear in Fig. 5a, before rain commences. One interpretation of these photographs might be that the clay is simply washed-out of the sand but recall the earlier

observation that both particle sizes are dispersed into the water upon drop impact. Again, these results agree with Rose's conceptual model.

5. Conclusion

The conceptual erosion model proposed by Rose is clearly applicable to the limiting experimental conditions used in this study. Because of the experimental simplicity and transparency of the design, it was possible to reduce the model to a few simple parameters, only one of which had to be experimentally obtained, namely the soil detachability, a. In particular, this research visually and quantitatively displays the formation of a "shield" during rain-impact erosion; this is a unique aspect of the Rose model not found in other erosion models and, thus, might prevent them from reproducing these experimental observations as readily as the Rose model. This is especially interesting in light of the apparent triviality of the experiments. Finally, the study obtained excellent quantitative agreement between the observations and the Rose model. Small discrepancies between the model and observations suggest further refinements to the model. The authors hope that other scientists with erosion models will attempt to see how well they can fit our data. Our next steps in this research include investigating the shielding mechanism in more detail and looking to spatial effects. We hope that the experimental set-up used in this study can be employed to measure actual soil detachability; this, of course, would require undisturbed soil samples and "natural rainfall."

References

Hairsine, P.B., Rose, C.W., 1991. Rainfall detachment and deposition: sediment transport in the absence of flow-driven processes. Soil Sci. Soc. Am. J. 55, 320–324.

Parlange, J.-Y., Hogarth, W.L., Rose, C.W., Sander, G.C., Hairsine, P., Lisle, I., 1999. Addendum to unsteady soil erosion model. J. Hydrol. 217, 149–156.

Proffitt, A.P.B., Rose, C.W., Hairsine, P.B., 1991. Rainfall detachment and deposition: experiments with low slopes and significant water depths. Soil Sci. Soc. Am. J. 55, 325–332.

Rose, C.W., Hogarth, W.L., Sander, G., Lisle, I., Hairsine, P., Parlange, J.-Y., 1994. Modeling processes of soil erosion by water. Trends Hydrol. 1, 443–451.

Sander, G.C., Hairsine, P.B., Rose, C.W., Cassidy, D., Parlange, J.-Y., Hogarth, W.L., Lisle, I.G., 1996. Unsteady soil erosion model, analytical solutions and comparison with experimental results. J. Hydrol. 178, 351–367.